Research Article

Thermally Radiative Flow of Non-Newtonian Fluid in an Inclined Channel Through Variable Permeability

Zaheer Abbas, Muhammad Saleem, Muhammad Yousuf Rafiq, Hafiz Shahzad* and Aqeel Ur Rehman

Department of Mathematics, The Islamia University of Bahawalpur, Bahawalpur 63100, Pakistan.

Abstract: This paper examines the thermally radiative Poiseuille flow of a non-Newtonian Jeffrey fluid through a porous medium with variable inclination and permeability. For simplification, let us assume that permeability varies in a quadratic parabolic form. The Brinkman model is applied to the porous medium to effectively regulate the flow. The impacts of viscous dissipation are also incorporated into the energy equation. The exact solution for velocity and temperature fields is obtained using the direct integration method, and then the obtained results are plotted to see the influence of different physical parameters. Furthermore, the skin friction coefficient and local Nusselt numbers are precisely calculated numerically for a variety of parameters, with the results presented comprehensively in tabular form. It is observed that the maximum permeability of the porous medium affects both the mass flow rate and the velocity, which increase with rising Jeffrey and decrease with rising Hartmann, number, respectively.

Received: September 11, 2024; **Accepted:** December 11, 2024; **Published:** December 21, 2024
***Correspondence:** Hafiz Shahzad, Department of Mathematics, The Islamia University of Bahawalpur, Bahawalpur 63100, Pakistan; **Email:** shahzad.gulzarr@gmail.com
Citation: Abbas, Z., M. Saleem, M.Y. Rafiq, H. Shahzad and A.U. Rehman. 2024. Thermally radiative flow of non-newtonian fluid in an inclined channel through variable permeability. *Journal of Engineering and Applied Sciences,* 43: 80-90.
DOI: https://dx.doi.org/10.17582/journal.jeas/43.80.90
Keywords: Poiseuille flow, Jeffrey fluid, Variable permeability, Heat transfer, Inclined channel, Exact solution

Introduction

In numerous physical situations, solid surfaces frequently exhibit wavy structures. For instance, mica cleavage surfaces display irregularities around 20 angstroms in size, while even smooth quartz crystals can have surface irregularities as tall as 100 angstroms. Recently, the investigation of flow dynamics near such irregular or wavy walls has garnered considerable attention due to its wide range of applications. A variety of subjects are covered by these applications, such as film vaporization in combustion chambers, cross-hatching on ablative surfaces, transpiration cooling for re-entry vehicles and rocket boosters, and engineering systems like heat exchangers and nuclear reactors. The fluid flow through porous surfaces, which is often resolved by applying an empirical slip-flow boundary constraint at these surfaces to match Darcy's Law with the Navier-Stokes equation (Neala and Nader, 1974). A criticism of the Brinkman-Forchheimer suitability for simulating flow in permeable media and at the edge between permeable medium and clear fluid (Nieid, 1991). A boundary layer around a vertical, flat plate was the subject of free convection (Rees and Pop, 1998). The stokes flow of an unsettled micropolar liquid between two isotropic

permeable panels (Srinivasacharya *et al*., 2001). An in-depth study on entropy generation in conduits packed with permeable media, considering both total and partial scenarios (Morosuk, 2005). Utilizing Brinkman's equation to explore three distinct flow patterns determined by Darcy number, tailoring the model equation for shallow porous layers accordingly (Parvazinia *et al*., 2006). The free conduction of extremely hydromagnetic viscoelastic fluid inside a vertical tube (Kumar *et al*., 2010). The homotopy evaluation method to examine the comportment of viscoelastic and hydromagnetic liquids near a vertical permeable region (Muthuraj and Srinivas, 2010). The oscillatory flow of an electrically conducting Casson fluid via a porous horizontal conduit under velocity slip constraints. Again, the Bödewadt flow of nanofluid across a spinning disk with heat and mass transport effects.

Biology and engineering both make substantial usage of investigational studies on non-Newtonian liquid dynamics. Conceptual research concentrates on physiological (polymer) liquids and non-Newtonian liquids such as blood. Non-Newtonian Jeffrey fluid models provide superior representations of physiological fluids, which has led many researchers to focus on these models (Hayat *et al*., 2006). A well-known Reynolds model to investigate the upshots of varying viscosity with Jeffrey liquid in a flexible media. In an asymmetrically inclined channel (Nadeem and Akbar, 2009). The effect of slip over the Jeffrey liquid peristaltic flow (Srinivas and Mathuraj, 2010). Assuming that blood acts as a Jeffrey fluid, scrutinized blood movement over a restricted tube (Akbar *et al*., 2011). Highlighted the influence of permeable media on the dynamics of Jeffrey fluids by concentrating on peristaltic movement with changing viscosity in an irregular conduit (Khan *et al*., 2012). Additionally, they looked into convective Couette movement in a conduit that slopes and has a porous wall on both sides. The unsteady movement of a magnetohydrodynamic Jeffrey liquid between equivalent walls lined with permeable material (Reddappa *et al*., 2024). Various scientific theories are proposed to explain the comportment of Jeffrey fluids below different constraints. The behavior of Jeffrey liquid in peristaltic flow through an asymmetric conduit (Abd-Alla and Abo Dahab, 2015). The movement characteristics of Jeffrey fluids in microscale tubes. Thermal investigation of blood flow down an inclined wavy channel driven by metachronal waves of cilia involving pseudo-plastic, dilatant, and Newtonian liquids was carried out (Al-Zubaidi *et al*., 2021). They discovered that for dilatant fluids, the velocity drops, but near channel walls, it exhibits the opposite behavior. For Newtonian and pseudo-plastic fluids, velocity grows in the center area of the conduit. Their investigation revealed that magnetic fields and slick barriers had opposing impacts on the dynamics of the flow. The behavior of a pair stress liquid in a sloped conduit was studied analytically (Ahmad *et al*., 2021). Effects of slip boundary constraints, magnetic forces, and permeable media on Jeffrey fluid flow (Nazeer *et al*., 2022). Considering entropy generation, the effect of an endoscope on the peristaltic flow of a Jeffery fluid in an annulus (Fayyaz *et al*., 2024). Various studies conducted in recent years are referenced in sources (Hamdan and Kamel, 2011; Anwer *et al*., 2020; Bandi *et al*., 2023; Mujahid *et al*., 2024; Shahzad *et al*., 2024).

The properties of heat transport are extensively utilized in various contexts, including thermal treatments, muscles, and skin tissues. Many researchers have conducted significant studies on heat transport within the human body, as it profoundly affects blood flow rates and subsequently alters physiological conditions. Understanding these fluid dynamics is essential for advancing technological innovations, operations, and efficiency across multiple fields. How changes in the temperature of the surrounding water affect blood flow variations (Barcroft and Edholm, 1943). The various complex numerical and analytical approximation methods available in the literature for estimating the temperature field over a porous fin (Turkyilmazoglu, 2017). For the rheology inside a long circular conduit, the Eyring-Powell fluid's non-Newtonian physical model (Turkyilmazoglu, 2020). Analytically examine the laminar flow and heat transfer characteristics of a viscous fluid around a long horizontal or vertical circular cylinder (Turkyilmazoglu, 2021). The focus on stagnation-point flow and heat transfer as it impinges on a stretchable flat plate or circular cylinder (Turkyilmazoglu, 2021). A computational examination of the time-dependent behavior of magnetohydrodynamic nanoparticles in mass and heat transfer, considering the effects of chemical reactions and heating elements (Li *et al*., 2022). Fractional non-singular simulations of radiation, mass, and heat transport processes using different slip and convection boundary effects (Raza *et al*., 2022). The mass and heat transfer dynamics of two non-mixable Jeffrey liquids flowing in a perpendicular

conduit (Kalyan *et al*., 2023). The effect of changing liquid characteristics on the MHD of viscous liquid peristaltic flow via a tapered conduit (Rafiq *et al*., 2024). The thin-film flow of a micropolar fluid over an inclined and dynamic substrate while being affected by heat and gravitational forces and including nanoparticles is stated as a physical problem (Siddiqui and Turkyilmazogluhg, 2024). Citations to some of the most pertinent studies on the topic of the investigation may be found in (Firdous *et al*., 2020; Asghar *et al*., 2022; Shahzad *et al*., 2024).

Most existing literature examines permeable media through stable permeability. We believe that incorporating varying permeability will be beneficial for studying flow through artificial porous media, such as in the strategy of synthetic examination of deformable bones and their structures materials. It is hypothesized that underground movement is affected by surrounding permeable layers with differing permeabilities. Based on these insights, we explored the flow of Jeffrey liquid in between two immovable barriers, an inclination conduit, considering both scenarios with and without variable porous media while applying a constant temperature to the wall. The goal of this study is to scrutinize the comparison of the impact of the permeability in an inclined conduit in the presence of heat. It gives a hypothetical foundation for exploring how permeability variations affect the way Jeffrey liquids move through permeable materials in a conduit that slopes. We examine three scenarios: (i) Poiseuille flow on an inclined plane over a permeable medium, (ii) Poiseuille flow in the absence of a permeable media on an inclined plane, and (iii) the influence of heat in both porous and non-porous media. In these cases, various input values are used to assess the equations for mass flow and velocity distribution. This research examines how classical Poiseuille flow between parallel plates is affected by tilt, the Jeffrey parameter, and varying permeability. The results of the numerical analysis are presented in tables and summaries, complemented by graphical representations showing the influence of key parameters on momentum, skin friction, and mass flow.

Mathematical analysis

Consider the thermally radiative Poiseuille flow of a non-Newtonian Jeffrey fluid fluid in a plane through a porous medium. The channel width is The permeability of the porous medium between the two solid walls in the infinite channel is examined under the assumption that the pressure gradient in the direction is constant. For the sake of argument, let the angle of the channel relative to the horizontal be θ as shown in Figure 1.

$$\boldsymbol{\tau} = -p\boldsymbol{I} + \boldsymbol{S}. \quad ...(1)$$

$$\boldsymbol{S} = \frac{\mu}{1+\lambda_1}(\dot{\overline{\gamma}} + \lambda_2 \ddot{\overline{\gamma}}). \ ...(2)$$

Where; S represent the extra stress tensor, τ denotes the Cauchy stress tensor, I is the identity tensor, p denotes pressure, λ_2 denotes the retardation time, λ_2 signifies the ratio of relaxation to retardation time, and ɣ is the shear rate. Dots signify derivative w.r.t to time. Consider The Brinkman equation Al-Zubaidi *et al*. (2021) and the continuity of steady Poiseuille flow in permeable media.

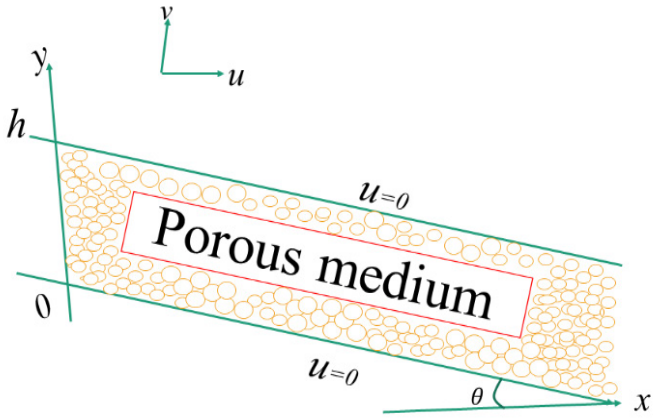

Figure 1: *Problem configuration.*

$$\frac{\partial \overline{u}}{\partial \overline{x}} = 0 \ ...(3)$$

$$\frac{\mu_{eff}}{1+\lambda_1}\frac{d^2\overline{u}}{d\overline{y}^2} - \frac{\mu}{k(y)}\overline{u} = \frac{\partial \overline{p}}{\partial \overline{x}} - \rho g \sin\theta \ ...(4)$$

$$\frac{\partial \overline{p}}{\partial \overline{x}} = -\rho g \cos\theta \quad ...(5)$$

$$k\frac{\partial^2 \overline{T}}{\partial \overline{y}^2} + \frac{\mu}{1+\lambda_1}\left(\frac{\partial \overline{u}}{\partial \overline{y}}\right)^2 - \frac{\partial q_y}{\partial \overline{y}} = 0 \ ...(6)$$

The boundary constraints are given as:

$$\begin{array}{llll} \overline{u}=0, & \overline{T}=T_0, & \text{at} & \overline{y}=0, \\ \overline{u}=0, & \overline{T}=T_1, & \text{at} & \overline{y}=h. \end{array} \ ...(7)$$

In the above equations, μ is the velocity in the x-direction, ρ is the fluid density, μ is the kinematic viscosity, g is the acceleration due to gravity, k is the thermal conductivity, and q_y is the radiative heat flux

and is given by:

$$q_y = -\frac{4\sigma^*}{3k^*}\frac{\partial T^4}{\partial \bar{y}} = -\frac{16\sigma^* T_0^3}{3k^*}\frac{\partial \bar{T}}{\partial \bar{y}} \ldots (8)$$

Let's examine the permeability equation in quadratic form, where the upper and inferior walls are kept at zero, the maximum permeation occurs over the straight middle line of the transmission (y = h/2) Supposing $k(y)= ay^2+by+c$, and the boundary constraints $k(0)= 0$, $k(h)=0$, we get the expansion for permeability as $k(y)= a(y-yh)$ where a is constant. Now $k(y)$ achieves maximum, say $k_{max}= -ah^2/4$ at y=h/2 So, $k(y)$ is in the form:

$$k(y) = \frac{-4k_{\max}}{h^2}(\bar{y} - h)y. \ldots (9)$$

$$\vartheta = \frac{\mu_{eff}}{\mu}, \quad Ha = \frac{h^2}{\vartheta k_{\max}}, \quad y = \frac{\bar{y}}{h}, \quad k = \frac{k(y)}{k_{\max}}, \quad u = \frac{\bar{u}}{u_{\max}},$$
$$p = \frac{\bar{p}}{\rho u^2_{\max}}, \quad x = \frac{\bar{x}}{h}, \quad \gamma = \frac{\bar{T} - T_0}{T_1 - T_0}. \ldots (10)$$

Substituting the non-dimensional quantities in Eqations 3-7, we get the following system of equations:

$$\frac{d^2u}{dy^2} - \frac{H_a(1\ \lambda_1)}{k(y)}u = -\frac{(1\ \lambda_1)\mathrm{Re}}{\vartheta}\left(P + \frac{\sin\theta}{Fr}\right). \ldots (11)$$

$$(1+R)\frac{\partial^2\gamma}{\partial y^2} + \frac{B_r}{1+\lambda_1}\left(\frac{\partial u}{\partial y}\right)^2 = 0. \ldots (12)$$

The dimensionless boundary conditions are given by:

$$u(0) = 0, \quad \gamma(0) = 0,$$
$$u(1) = 0, \quad \gamma(1) = 1. \ldots (13)$$

In the above equations, Fr=u^2_{max}/gh is the Froude number, Re=ρumaxh/u is the Reynolds number, R=16σ*T3∞/3k*k is the thermal radiation parameter, Br=μu2max/k(T1-T0) is the Brinkman number and P= δp/δx. The permeability variables are given by:

$$k(y) = -4(y^2 - y) \ldots (14)$$

Materials and Methods

For porous medium

The suitable solution for Equation 11 with boundary constraints are given as:

$$u = A(y^2 - y). \ldots (15)$$

Utilizing Equations 14 and 15 in 9 and 10, we obtain:

$$u = \frac{-4(1+\lambda_1)\mathrm{Re}\left(P + \frac{\sin\theta}{Fr}\right)}{\vartheta(8 + H_a(1+\lambda_1)}(y^2 - y) \ldots (16)$$

$$\gamma = y - \frac{A^2 B_r (y^2 - y)\left(1 + 2(y^2 - y)\right)}{6(1+R)(1+\lambda_1)} \ldots (17)$$

Where; $A = -\frac{4(1+\lambda_1)\mathrm{Re}\left(P + \frac{\sin\theta}{Fr}\right)}{\vartheta(8 + H_a(1+\lambda_1)}$.

For non-porous medium

The governing equations for a non-porous medium are given by:

$$\frac{1}{1+\lambda_1}\frac{d^2\bar{v}}{d\bar{y}^2} = \frac{1}{\mu}\frac{d\bar{p}_1}{d\bar{x}} - \frac{\rho g \sin\theta}{\mu} \ldots (18)$$

$$k\frac{\partial^2\bar{T}}{\partial\bar{y}^2} + \frac{\mu}{1+\lambda_1}\left(\frac{\partial\bar{v}}{\partial\bar{y}}\right)^2 - \frac{\partial q_y}{\partial\bar{y}} = 0 \ldots (19)$$

The boundary conditions are given by:

$$\bar{v} = 0, \quad \bar{T} = T_0, \quad \text{at} \quad \bar{y} = 0,$$
$$\bar{v} = 0, \quad \bar{T} = T_1, \quad \text{at} \quad \bar{y} = h. \ldots (20)$$

Non-dimensional quantities are:

$$\bar{v} = \frac{v}{v_{\max}}, \quad \bar{x} = \frac{x}{h}, \quad \bar{y} = \frac{y}{h}, \quad \bar{p}_1 = \frac{p_1}{\rho v^2_{\max}}, \quad \gamma = \frac{\bar{T} - T_0}{T_1 - T_0} \ldots (21)$$

Utilizing non-dimensional quantities, the governing equations and boundary constraints transform into:

$$\frac{d^2v}{dy^2} = -(1+\lambda_1)\mathrm{Re}\left(P_1 + \frac{\mathrm{Sin}\,\theta}{Fr}\right) \ldots (22)$$

$$(1+R)\frac{\partial^2\gamma}{\partial y^2} + \frac{B_r}{1+\lambda_1}\left(\frac{\partial v}{\partial y}\right)^2 = 0 \ldots (23)$$

$$v(0) = 0, \quad \gamma(0) = 0, \quad v(1) = 0, \quad \gamma(1) = 1. \ldots (24)$$

Where Re=ρvmaxh/μ is the Reynolds number, Fr=v^2_{max}/gh is the Froude number and P1= δp/δx.

The solution of velocity and temperature is given by:

$$v = -\frac{1}{2}(1+\lambda_1)(y^2 - y)\mathrm{Re}\left(P_1 + \frac{\sin\theta}{Fr}\right). \ldots (25)$$

$$\gamma = y - \frac{A^2 B_r (y^2 - y)\left(1 + 2(y^2 - y)\right)}{6(1+R)(1+\lambda_1)} \ldots (26)$$

$$\text{Where; } A = -\frac{1}{2}(1+\lambda_1)\,\mathrm{Re}\left(P_1 + \frac{\sin\theta}{Fr}\right) \ldots (27)$$

Mass flux

As a function of conduit length, the dimensionless mass flux for Poiseuille flow over a permeable media on an inclined plane is represented as:

$$M_1 = \int_0^1 u\,dy = \frac{A}{6} \ldots (28)$$

The mass flux on slanted planes under Poiseuille flow in the non-porous medium.

$$M_2 = \int_0^1 v\,dy = \frac{1}{12}(1+\lambda)\,\mathrm{Re}\left(P_1 + \frac{\sin\theta}{Fr}\right) \ldots (29)$$

Skin friction

The skin friction at y=1 is given by the relation:

$$\left|\tau_{yx}\right| = \frac{\vartheta}{\mathrm{Re}(1+\lambda_1)}\frac{du}{dy} = \frac{4}{8+H_a(1+\lambda_1)}\left(P + \frac{\sin\theta}{Fr}\right) \ldots (30)$$

Nusselt number

The Nusselt number at y=1 is given by:

$$Nu = -(1+R)\frac{d\gamma}{dy} \ldots (31)$$

Result and Discussion

In the subsequent subsections, we focus on the mechanism to control the velocity, temperature, and Mass flux through variations of the characterizing parameters such as the Froude number ($0 \le Fr \le 1$), Jeffrey parameter ($0 \le \lambda 1 \le 1$), Reynolds number ($1 \le Re \le 50$), pressure gradient ($0.3 \le P \le 1$), angle of inclination ($0 \le \theta \le 2$), and Brinkman number ($0 \le Br \le 10$). These parameter values are designated according to the previous literature Anwar-bag *et al.* (2020), Rafiq *et al.* (2024), Siddiqui and Turkyilmazoglu (2024) and Firdous *et al.* (2020) and these are beneficial for experimental purposes. Performing a comparative analysis between the present study and the previously published paper is a valuable approach to validating the accuracy of the present results. The close agreement between the outcomes of the present study and the existing literature confirms the accuracy and reliability of the present results as shown in Table 1. Table 2 provides the variation in Nusselt number for different physical parameters. In graphs, solid lines are used for porous medium, and dashed lines are used for non-porous medium. The model algorithm is shown in **Figure 2**.

Table 1: *Comparison of skin friction $|C_f|$ at y=1 with that of Bandi et al. (2023) with λ1= 0.5, P = 3, θ = π/6, Ha =1.*

	Fr	0.1	0.2	0.3	0.4	0.5
Bandi *et al.* (2023)	$\|C_f\|$	3.28	2.29	1.97	1.77	1.67
Present study	$\|C_f\|$	3.37	2.31	1.96	1.79	1.69

Table 2: *Effect of Nusselt number coefficient for distinct physical parameters.*

Parameters				Nusselt Number Nu	
Fr	R	B_r	Λ1	Non-Porous	Porous
0.1	0.4	2	1.5	1.0928	0.5467
0.2				1.2548	0.9967
0.3				1.2955	1.1096
	0.2			1.0548	1.0991
	0.4			1.2548	0.9967
	0.6			1.4548	0.6925
		1		1.2548	0.9967
		5		0.6740	0.6333
		10		0.0012	0.0061
			1	1.2548	0.9967
			2	1.2200	0.7950
			3	1.1983	0.5933

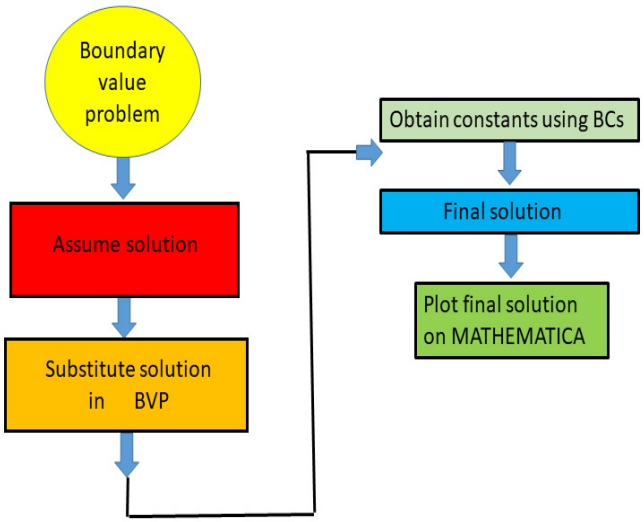

Figure 2: *Model algorithm.*

The effects of various parameters on the velocity profile in porous medium and non-porous medium are shown in Figsures 3-7. The influence of Fr on the velocity profile is depicted in Figure 3. Figure 3 demonstrates that the fluid velocity diminutions in both mediums by enhancing the values of Fr. As the Froude number increases, the influence of gravity becomes more pronounced in relation to the fluid's inertia. This leads to a stronger downward or stabilizing effect on the fluid. Consequently, the fluid

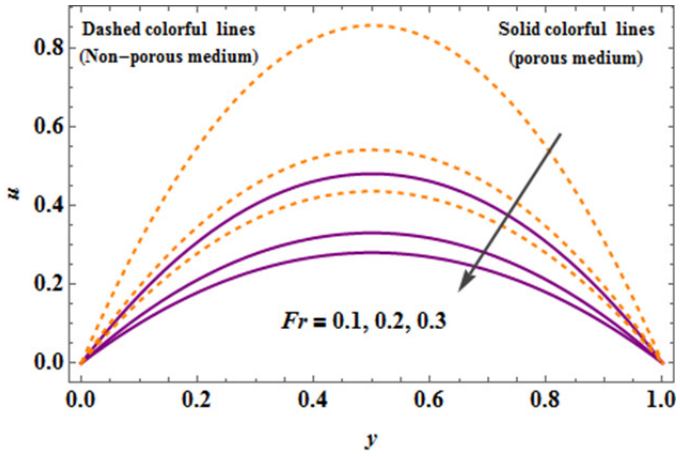

Figure 3: *Velocity profile for distinct values of Fr.*

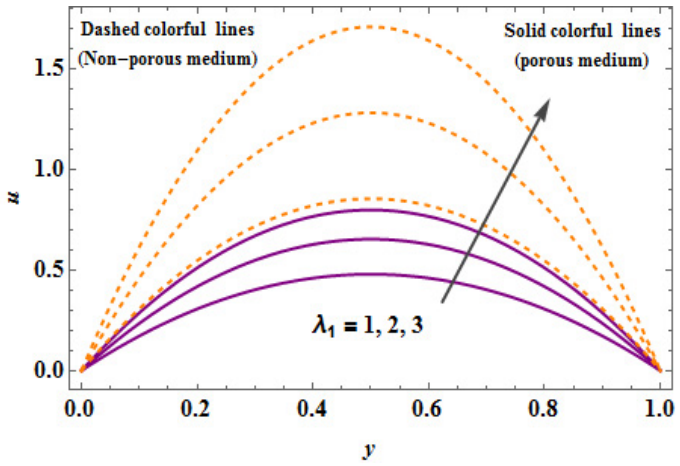

Figure 4: *Velocity profile for distinct values of* λ_1.

experiences an increased resistance to its motion due to gravity, which opposes the inertia-driven movement of the fluid. As a result, the overall fluid velocity decreases when the Froude number increases. The deviation in velocity profile for various values of Jeffrey fluid parameter is exhibited in Figure 4. This graph indicates that the liquid velocity is enhanced by enhancing the λ1. The Jeffrey fluid model modifies the constitutive equation to account for elasticity effects, often leading to the fluid responding more elastically to applied forces. When the Jeffrey parameter increases, the fluid exhibits more elastic behavior. In peristaltic or channel flows, this elasticity allows the fluid to store and release energy more effectively as it moves, which reduces resistance to flow and promotes higher fluid velocity. The dimensional velocity profiles increase the velocity in the porous layer, the channel, and the rate at the interface at increasing driving pressure gradient values for a given viscosity. It is important to note that for all pressure gradient values; the chosen permeability distribution yields smoothly shifting velocity profiles (Figure 5). The viscous forces become less significant as the Reynolds number rises, and velocity defects in the flow field will propagate less. The wall shear stress is decreased at higher Reynolds numbers because less fluid is dragged along the surface. Figures 6 and 7 demonstrate how velocity rises with increasing Re and θ. As compared to a non-porous media, the results show that the Poiseuille flow of a non-Newtonian liquid in a heated permeable conduit with variable absorbency decreases velocity in the permeable medium. In a porous medium, the velocity profile tends to decrease compared to a non-porous layer due to the increased resistance created by the medium's permeability. As fluid flows through a porous structure, the material obstructs its movement, generating drag forces that dissipate kinetic energy and slow the flow rate. This resistance, often represented through Darcy's law or similar terms, reduces the overall velocity within the porous layer.

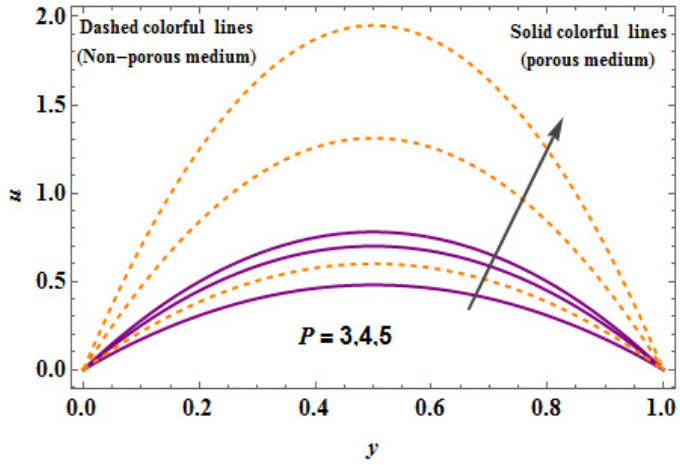

Figure 5: *Velocity profile for distinct values of P.*

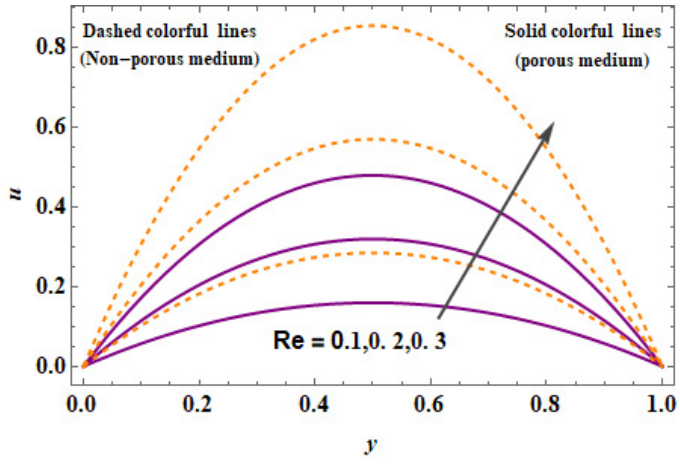

Figure 6: *Velocity profile for distinct values of Re.*

Figure 8 is plotted to see the deviations in mass flux M1 and M2 against λ1 for dissimilar values of Re. This graph indicates that the max flux is enhanced by increasing the values of Ha. The impact of the

inclination angle θ on the mass flux M1 and M2 against λ1 is depicted in Figure 9 and observed that the mass flux is augmented by augmenting the values of θ. Figure 10 illustrates that the mass flow drops as the Froude number upsurges.

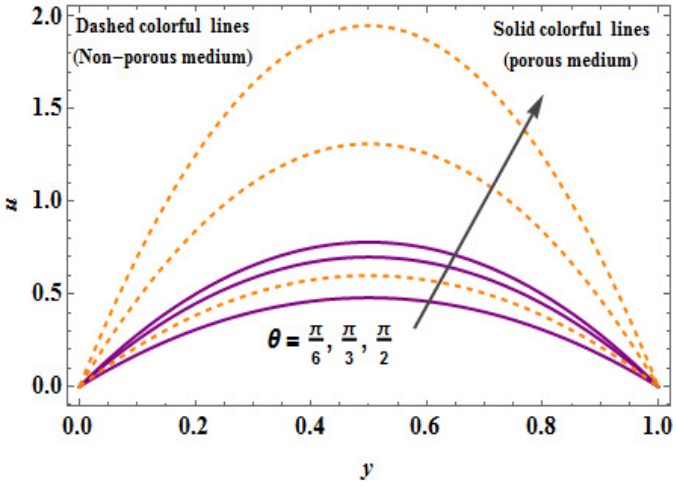

Figure 7: *Velocity profile for distinct values of θ.*

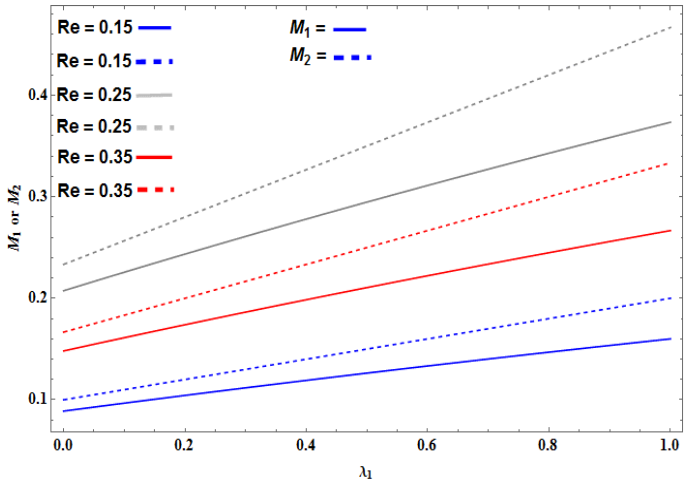

Figure 8: *Mass flux variation with λ_1 for distinct value of Re.*

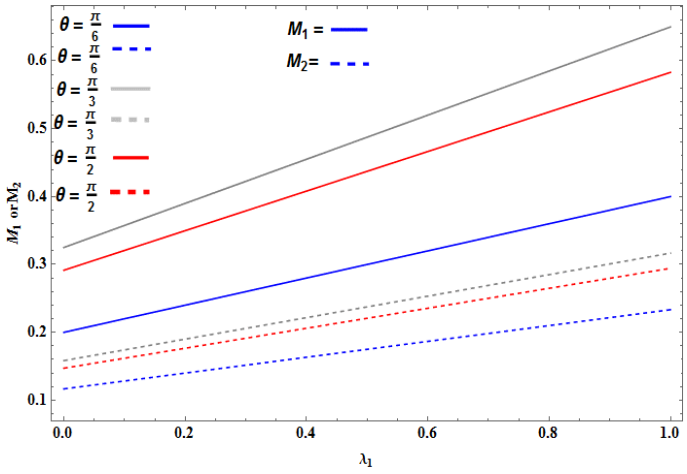

Figure 9: *Mass flux variation with λ_1 for distinct value of θ.*

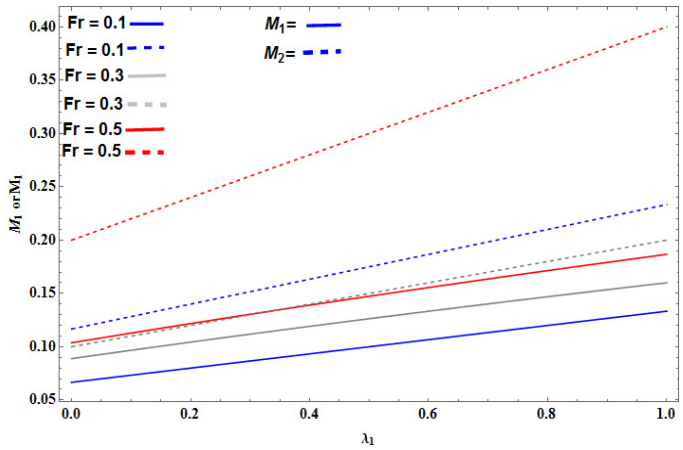

Figure 10: *Mass flux variation with λ_1 for distinct value of Fr.*

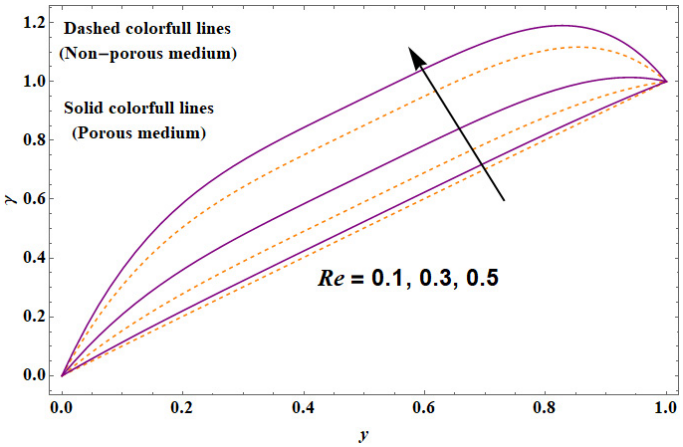

Figure 11: *Temperature profile for distinct values of Re.*

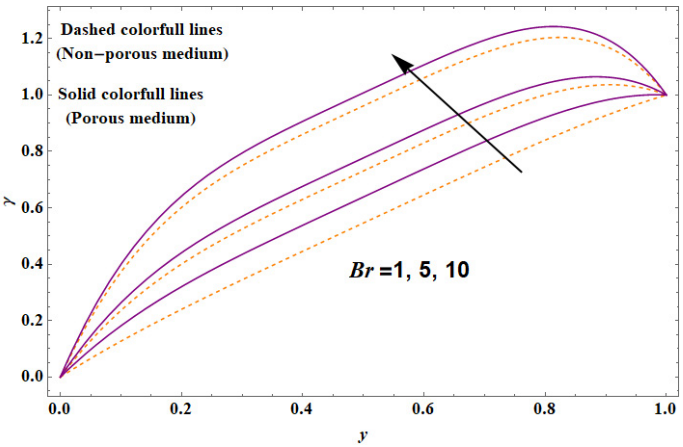

Figure 12: *Temperature profile for distinct values of Br.*

Figures 11-13 are plotted to depict the deviations in temperature profile for various values of the Reynold number Re, Jeffrey parameter λ1, and Brinkman number Br. The heat transfer is increased in a porous medium in comparison to a non-porous medium. Figure 11 illustrates the influence of the Reynolds number Re on the thermal profile γ. It can be noted the liquid temperature is increased by augmenting the values of Re. Figure 12 shows that the temperature

profile is upsurged by enhancing values of the Brinkman number Br. Physically, a higher Brinkman number indicates a greater influence of viscous dissipation, where the kinetic energy of fluid motion is converted into thermal energy due to internal friction. This conversion generates additional heat within the fluid, causing a rise in temperature. As the Brinkman number increases, the amount of heat generated from viscous dissipation becomes more significant, which enhances the overall temperature of the fluid. The impact of λ1 on the temperature profile is displayed in Figure 13. A significant upsurge in the temperature profile can be observed when λ1 is increased. The impact of dissimilar parameters on the Nusselt number is shown in Table 2. It can be concluded from this table that the Nusselt number is enhanced by enhancing the values of Fr and R however, it is decreased by increasing the values of Br and λ1.

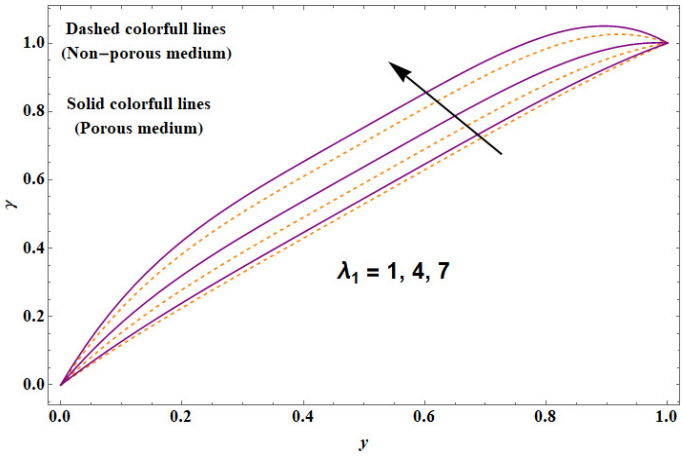

Figure 13: *Temperature profile for distinct values of λ.*

Conclusions and Recommendations

This paper investigates the dynamics of non-Newtonian Jeffrey fluid flow along an inclined heterogeneous heated porous and non-porous stratum. The profile is associated with a smooth permeability function, which mitigates permeability discontinuities near the solid, bounding walls. The key findings of the study are:

- The velocity of the fluid upsurges with higher values of the Jeffrey parameter, Reynolds numbers, and inclination angle.
- The velocity profile in the porous stratum decreases as compared with the non-porous stratum.
- An increase in the Jeffrey parameter enhances the mass flux in the conduit, while an increase in the variable Hamdan number exhibits the opposite effect.
- An upsurge in the values of the Jeffrey parameter increases the thickness of the momentum boundary layer.
- The fluid temperature is augmented with higher values of the Jeffrey parameter, Reynolds numbers, and Brinkman number.

Acknowledgement

We are thankful to the reviewers for their encouraging comments and constructive suggestions to improve the quality of the manuscript.

Novelty Statement

This study presents a novel analytical investigation of thermally radiative Poiseuille flow of a Jeffrey fluid through a porous medium with variable inclination and quadratic permeability, incorporating the Brinkman model and viscous dissipation effects to derive exact solutions for velocity and temperature fields.

Authors Contribution

Zaheer Abbas: Conceptualization, Investigation, Project administration, Resources, Supervision.
Muhammad Saleem: Formal analysis, Methodology, Investigation, Data curation, Software, Writing original draft.
Muhammad Yousuf Rafiq: Writing review and editing, visualization, validation, software, methodology, conceptualization.
Muhammad Yousuf Rafiq: Conceptualization. Validation, Visualization, Investigation, Writing–review & editing.
Hafiz Shahzad and Aqeel Ur Rehman: Software, Visualization, Data curation, Writing–review & editing.

Conflict of interest
The authors declare that they have no known competing financial interests or personal relationships that could have appeared to influence the work reported in this paper.

References

Abbas, Z., M.S. Arslan, M.Y. Rafiq and J. Hasnain. 2022. Mass transfer in magnetohydrodynamic oscillatory flow of casson liquid through a

porous horizontal channel with velocity slip. Biosens. Nanotheranost., 1(1): 1-13, 9823. https://doi.org/10.25163/biosensors.119823

Abbas, Z., S. Siddique, M.Y. Rafiq and A.U. Rehman. 2023. On generalized Bödewadt flow of TiO2/water nanofluid over a permeable surface with temperature jump. Adv. Mech. Eng.. 15(10): 16878132231201299. https://doi.org/10.1177/16878132231201299

Abd-Alla, A.M. and S.M. Abo-Dahab. 2015. Magnetic field and rotation effects on peristaltic transport of a Jeffrey fluid in an asymmetric channel. J. Magnet. Magnet. Mater., 374: 680-689. https://doi.org/10.1016/j.jmmm.2014.08.091

Khan, A.A., R. Ellahi and K. Vafai. 2012. Peristaltic transport of a Jeffrey fluid with variable viscosity through a porous medium in an asymmetric channel. Adv. Mathemat. Phys., 2012(1): 169642. https://doi.org/10.1155/2012/169642

Ahmad, F., M. Nazeer, W. Ali, A. Saleem, H. Sarwar, S. Suleman and Z. Abdelmalek. 2021. Analytical study on couple stress fluid in an inclined channel. Sci. Iranica, 28(4): 2164-2175.

Akbar, N.S., S. Nadeem and M. Ali. 2011. Jeffrey fluid model for blood flow through a tapered artery with a stenosis. J. Mech. Med. Biol., 11(3): 529-545. https://doi.org/10.1142/S0219519411003879

Al-Zubaidi, A., M. Nazeer, K. Khalid, S. Yaseen, S. Saleem and F. Hussain. 2021. Thermal analysis of blood flow of Newtonian, pseudo-plastic, and dilatant fluids through an inclined wavy channel due to metachronal wave of cilia. Adv. Mech. Eng., 13(9): 16878140211049060. https://doi.org/10.1177/16878140211049060

Anwar-Beg, O., M. Ferdows, M.E. Karim, M.M. Hasan, T.A. Bég, M.D. Shamshuddin and A. Kadir, 2020. Computation of non-isothermal thermo-convective micropolar fluid dynamics in a Hall MHD generator system with non-linear distending wall. Int. J. Appl. Comput. Mathemat., 6: 1-44. https://doi.org/10.1007/s40819-020-0792-y

Asghar, Z., M.W.S. Khan, M.A. Gondal and A. Ghaffari. 2022. Channel flow of non-newtonian fluid due to peristalsis under external electric and magnetic field. Proc. Inst. Mech. Eng. E: J. Process Mech. Eng., 236(6): 2670-2678. https://doi.org/10.1177/09544089221097693

Bandi, R., B.S. Mallela, S. Sreedharamalle and D. Putta. 2023. The flow of non-newtonian fluid in an inclined channel through variable permeability. Heat Transfer, 52(4): 3058-3073. https://doi.org/10.1002/htj.22816

Barcroft, H. and O.G. Edholm. 1943. The effect of temperature on blood flow and deep temperature in the human forearm. J. Physiol., 102(1): 5. https://doi.org/10.1113/jphysiol.1943.sp004009

Fayyaz, A., Z. Abbas and M.Y. Rafiq. 2024. Dynamics of thermal radiatively Jeffrey fluid through an annulus region between two flexible tubes with entropy generation. Phys. Scripta, 99(10): 105269. https://doi.org/10.1088/1402-4896/ad7997

Firdous, H., S.M. Husnine, F. Hussain and M. Nazeer. 2020. Velocity and thermal slip effects on two-phase flow of MHD Jeffrey fluid with the suspension of tiny metallic particles. Phys. Scripta, 96(2): 025803. https://doi.org/10.1088/1402-4896/abcff0

Hamdan, M.H. and M.T. Kamel. 2011. Flow through variable permeability porous layers. Adv. Theor. Appl. Mech., 4(3): 135-145. https://doi.org/10.1615/SpecialTopicsRevPorousMedia.v2.i2.80

Hayat, T., N. Ali, S. Asghar and A.M. Siddiqui. 2006. Exact peristaltic flow in tubes with an endoscope. Appl. Mathemat. Comput., 182(1): 359-368. https://doi.org/10.1016/j.amc.2006.02.052

Kalyan, S., A. Sharan and A.J. Chamkha. 2023. Heat and mass transfer of two immiscible flows of Jeffrey fluid in a vertical channel. Heat Transfer, 52(1): 267-288. https://doi.org/10.1002/htj.22694

Kumar, J.P., J.C. Umavathi, A.J. Chamkha and I. Pop. 2010. Fully-developed free-convective flow of micropolar and viscous fluids in a vertical channel. Appl. Math. Model., 34(5): 1175-1186. https://doi.org/10.1016/j.apm.2009.08.007

Li, Y.X., S.R. Mishra, P.K. Pattnaik, S. Baag, Y.M. Li, M.I. Khan, N.B. Khan, M.K. Alaoui and S.U. Khan. 2022. Numerical treatment of time dependent magnetohydrodynamic nanofluid flow of mass and heat transport subject to chemical reaction and heat source. Alex. Eng. J., 61(3): 2484-2491. https://doi.org/10.1016/j.aej.2021.07.030

Morosuk, T.V., 2005. Entropy generation in conduits filled with porous medium totally

and partially. Int. J. Heat Mass Transfer, 48(12): 2548-2560. https://doi.org/10.1016/j.ijheatmasstransfer.2005.01.018

Mujahid, M., Z. Abbas and M.Y. Rafiq. 2024. Rheological analysis of pressure-driven Jeffrey fluid flow between corrugated porous curved walls with slip constraints. AIP Adv., 14(9): 095122. https://doi.org/10.1063/5.0230681

Muthuraj, R. and S. Srinivas. 2010. Fully developed MHD flow of a micropolar and viscous fluids in a vertical porous space using HAM. Int. J. Appl. Math. Mech., 6(11): 55-78.

Nadeem, S. and N.S. Akbar. 2009. Peristaltic flow of a Jeffrey fluid with variable viscosity in an asymmetric channel. Zeitschrift für Naturforschung A., 64(11): 713-722. https://doi.org/10.1515/zna-2009-1107

Nazeer, M., A.A.A. Ahamdi, A.N. Alzaed, M. Alwetaishi, M.W. Nazir and M.I. Khan. 2022. Impact of slip boundary conditions, magnetic force, and porous medium on blood flow of Jeffrey fluid. ZAMM J. Appl. Math. Mech. Z. Angewandte Mathematik Mechanik, 102(10): 202100218. https://doi.org/10.1002/zamm.202100218

Neale, G. and W. Nader. 1974. Practical significance of Brinkman's extension of Darcy's law: Coupled parallel flows within a channel and a bounding porous medium. Can. J. Chem. Eng., 52(4): 475-478. https://doi.org/10.1002/cjce.5450520407

Nield, D.A., 1991. The limitations of the Brinkman-Forchheimer equation in modeling flow in a saturated porous medium and at an interface. Int. J. Heat Fluid Flow, 12(3): 269-272. https://doi.org/10.1016/0142-727X(91)90062-Z

Parvazinia, M., V. Nassehi, R.J. Wakeman and M.H.R. Ghoreishy. 2006. Finite element modelling of flow through a porous medium between two parallel plates using the Brinkman equation. Transport Porous Media, 63: 71-90. https://doi.org/10.1007/s11242-005-2721-2

Rafiq, M.Y., Z. Abbas, J. Hasnain and S. Khaliq. 2024. Insight into the peristaltic motion through a tapered channel with Newton's cooling subject to viscous dissipation, Lorentz force, and velocity slip. Adv. Mech. Eng., 16(4): 16878132241241436. https://doi.org/10.1177/16878132241241436

Raza, A., A. Ghaffari, S.U. Khan, A.U. Haq, M.I. Khan and M.R. Khan. 2022. Non-singular fractional computations for the radiative heat and mass transfer phenomenon subject to mixed convection and slip boundary effects. Chaos, Solitons Fractals, 155: 111708. https://doi.org/10.1016/j.chaos.2021.111708

Reddappa, B., R. Geetha, B.R. Kumar, M. Akermi, M.I. Khan and I. Khan,. 2024. Nonlinear coupled ODEs for nanofluid flow and heat transfer with varying thickness: A comparative study. Numer. Heat Transfer, B: Fundament., 25: 1-25. https://doi.org/10.1080/10407790.2024.2333013

Rees, D.A.S and I. Pop. 1998. Free convection boundary-layer flow of a micropolar fluid from a vertical flat plate. IMA J. Appl. Mathemat., 61(2): 179-197. https://doi.org/10.1093/imamat/61.2.179

Santhosh, N. and G. Radhakrishnamacharya. 2013. Flow of Jeffrey fluid through narrow tubes. Int. J. Sci. Eng. Res., 4: 468-473.

Shahzad, H., Z. Abbas and M.Y. Rafiq. 2024. Molecular dynamics study of the thermal radiatively pressure-driven flow of two immiscible hybrid nanofluids through a curved pipe with viscous dissipation. Chaos, Solit. Fractals, 188: 115552. https://doi.org/10.1016/j.chaos.2024.115552

Shahzad, H., Z. Abbas and M.Y. Rafiq. 2024. Rheological impact of viscous fluid in the core region of heated curved pipe surrounded by Casson rheological fluid. Case Stud. Thermal Eng., 61: 105156. https://doi.org/10.1016/j.csite.2024.105156

Siddiqui, A.A. and M. Turkyilmazoglu. 2024. Film flow of nano-micropolar fluid with dissipation effect. Comput. Model Eng. Sci., 140(3): 2487-2512. https://doi.org/10.32604/cmes.2024.050525

Srinivas, S. and R. Muthuraj. 2010. Peristaltic transport of a Jeffrey fluid under the effect of slip in an inclined asymmetric channel. Int. J. Appl. Mech., 2(2): 437-455. https://doi.org/10.1142/S1758825110000573

Srinivasacharya, D., J.R. Murthyand, D. Venugopalam. 2001. Unsteady stokes flow of micropolar fluid between two parallel porous plates. Int. J. Eng. Sci., 39(14): 1557-1563. https://doi.org/10.1016/S0020-7225(01)00027-1

Turkyilmazoglu, M., 2017. A direct solution of temperature field and physical quantities for the nonlinear porous fin problem. Int. J. Numer.

Methods Heat Fluid Flow, 27(2): 516-529. https://doi.org/10.1108/HFF-11-2015-0475

Turkyilmazoglu, M., 2020. Eyring–powell fluid flow through a circular pipe and heat transfer: Full solutions. Int. J. Numer. Methods Heat Fluid Flow, 30(11): 4765-4774. https://doi.org/10.1108/HFF-12-2019-0925

Turkyilmazoglu, M., 2021. Exact solutions concerning momentum and thermal fields induced by a long circular cylinder. Eur. Phys. J. Plus, 136(5): 1-10. https://doi.org/10.1140/epjp/s13360-021-01500-1

Turkyilmazoglu, M., 2021. Stagnation-point flow and heat transfer over stretchable plates and cylinders with an oncoming flow: Exact solutions. Chem. Eng. Sci., 238: 116596. https://doi.org/10.1016/j.ces.2021.116596